Turkish Journal of Science & Technology
19(2), 407-414, 2024

Research Paper
https://doi.org/10.55525/tjst.1459356

Variations in Diffusion Coefficients on Equinox Days at Specified Critical Heights of the Ionosphere at the Equator

Kadri KURT[1*], Ali YEŞİL[2]

[1]Elektrik ve Enerji Bölümü, Beşiri OSB Vocational School, Batman University, Batman, Turkey
[2] Yüksek Enerji ve Plazma Fiziği Bölümü, Fen Fakültesi, Fırat Üniversitesi, Elazığ, Turkey
[*1]kadridewani@gmail.com, [2]ayesil@firat.edu.tr

(Geliş/Received: 26/03/2024; Kabul/Accepted: 10/09/2024)

Abstract: This study investigates the local time diffusion coefficient for stable and unstable ($\omega = 0$, $\omega \neq 0$) states at the equator (0^0), "the geographical latitude where the first peak of the magnetic equatorial trough in the ionosphere occurs," during the spring and fall equinoxes (March 21 and September 23). The findings show that the diffusion tensor in a steady state is completely real and has a magnitude equal to the speed of light in a steady state. But in the unsteady state, the diffusion tensor consists of two parts, real and imaginary. The diagonal elements of the real part tensor are of the size of the conductivity in the ionosphere and the elements of the imaginary part are of the size of the speed of sound with about the same magnitude. Furthermore, for all assumed conditions, the diffusion elements form the first peak of the magnetic equatorial trough at 6.00 am local time.

Key words: Diffusion tensor, ionospheric plasma, diffusion coefficient.

Ekvatorda Iyonosferin Bazı Kritik Yüksekliklerinde Difüzyon Katsayılarının Ekinoks Günlerinde Değişimi

Öz: Bu çalışmada, ilkbahar ve sonbahar ekinoksları (21 Mart ve 23 Eylül) sırasında "iyonosferdeki manyetik ekvatoral çukurun ilk zirvesinin meydana geldiği coğrafi enlem" olan ekvatorda (0^0) kararlı ve kararsız ($\omega = 0$, $\omega \neq 0$) durumlar için yerel zaman zaman difüzyon katsayısı araştırılmıştır. Bulgulara göre, kararlı durumda difüzyon tensörünün tamamen gerçek olduğunu ve sabit bir durumda ışık hızına eşit bir büyüklüğe sahip olduğunu göstermektedir. Fakat kararsız durumda difüzyon tensörü; reel ve sanal olmak üzere iki kısımdan oluşmaktadır. Reel kısım tensörününün köşegen elemanları iyonosferdeki büyüklüğü iletkenlik boyutunda, sanal kısmının elamanları yaklaşık aynı büyüklükte ses hızı boyutundadır. Bunun yanı sıra bütün kabul edilen şartlarda difüzyon elemanları sabah 6.00'da yerel zamanda manyetik ekvator çukurun ilk tepesini oluşturmaktadır.

Anahtar kelimeler: Difüzyon tensörü, iyonosferik plazma, difüzyon katsayıları.

1. Introduction

A section of Earth's upper atmosphere that lies between 50 and 1000 kilometers above the surface of the Earth is known as the ionosphere. Solar energy, especially ultraviolet (UV) rays, ionizes this area [1,2]. The transmission and propagation of radio waves depend heavily on the ionosphere. The D, E, and F layers are among the layers that make up the ionosphere [3,4]. Ionized particles, also known as ions, are present in these layers and are produced when solar radiation removes electrons from neutral atoms and molecules [5]. Radio communication, satellite operations, and space weather prediction are just a few of the uses that depend on understanding the ionosphere and its fluctuations. To track and investigate the behavior of the ionosphere and its interactions with solar radiation, scientists and researchers utilize equipment like satellites and ionosondes. Neutral winds, geomagnetic activity, solar radiation, and other factors all have an impact on the complicated phenomenon of electron density change in the magnetic equatorial trough of the ionosphere. There are significant variations in the electron density profile of the ionosphere in the magnetic equatorial trough during the day, with daytime and nighttime differences being particularly noticeable [6]. The strong ultraviolet (UV) radiation from the Sun ionizes the neutral particles in the ionosphere's F region during the day, releasing free electrons and ions. The overall electron density in the F region is influenced by this process [7]. A major contributor is the eastward-directed electric current known as the Equatorial Electrojet, which flows close to the magnetic equator. Higher altitudes of ionized particles are transported by the upward **E**×**B** drift, which is facilitated by the electrojet. This may cause the electron density in the F region to increase, resulting in the formation of a peak near the magnetic equator [8]. One important driver is the **E**×**B** drift, which is caused by the interaction of the ionospheric magnetic field (**B**) and

* Corresponding author:kadridewani@gmail.com ORCID Number of authors: [1]0000-0002-6507-8234, [2]0000-0003-2997-897X

the Earth's electric field (**E**) [9]. The plasma moves vertically as a result of this drift and in some circumstances, it may cause the electron density profile to trough close to the magnetic equator. The electron density distribution is also influenced by the meridional (north-south) wind patterns. Meridional winds and the **E**x**B** drift can push ionized particles away from the magnetic equator, which can aid in the creation of the trough [10]. At night, when solar ionization is lower, recombination activities take center stage. Electron density decreases as a result of electron-neutral collisions. The trough may also occur as a result of loss processes such as gravity settling and ambipolar diffusion.

The electron density profile might trough at proximity to the magnetic equator as a result of it. The meridional (north-south) wind patterns have an impact on the electron density distribution as well. The trough may form as a result of ionized particles being pushed away from the magnetic equator by meridian winds and the **E**x**B** drift [11]. Nighttime brings more prominence to recombination events due to decreased solar ionization. Electron-neutral collisions result in a drop in electron density. Additionally, loss processes including ambipolar diffusion and gravity settling may cause a decrease.

2. Diffusion Equations for Steady(ω=0) and Unstable State($\omega\neq$0) Ionosphere Plasma

Given that the ionosphere's density inhomogeneity causes very minor departures from the equilibrium state and that these density instabilities are first-order, the velocity distribution can be roughly regarded as isotropic [12]. Density in this instance has the following definition. On the other hand, the medium is said to be anisotropic when **B** (magnetic field)≠0. There is not an isotropic velocity distribution. The ionospheric plasma is anisotropic because the magnetic field in the ionosphere plasma differs from zero [13,14]. As seen in Figure 1, the Earth's magnetic field takes on three dimensions when its true geometry is applied.

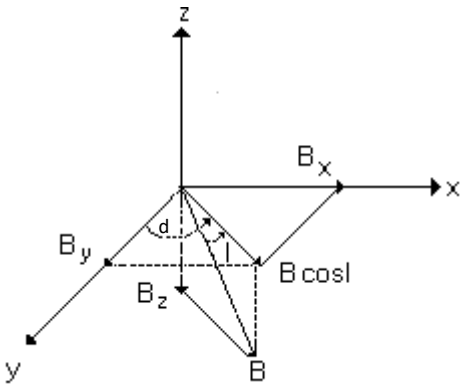

Figure 1. Geometry of the Earth's magnetic field (for the Northern Hemisphere) [2,14,15].

Here, $B_x = BCosISind$, $B_y = BCosICosd$ and, I is the magnetic dip and d is the magnetic declination angle. Other rotations to be used in this study are as follows:

ω_c: Electron Cyclotron (rotation) frequency. These frequencies depend on plasma parameters; is given as [2,14,15]

$$\omega_{cx\alpha} = \frac{eB_x}{m},\ \omega_{cy\alpha} = \frac{eB_y}{m} \text{ ve } \omega_{cz\alpha} = \frac{eB_z}{m}$$

If the geometry of the Earth's magnetic field is used in the flux density for the northern hemisphere, the diffusion equation can be written as follows;

$$\boldsymbol{\Gamma} + \frac{n_\alpha}{\nu_\alpha}\frac{D\mathbf{U}}{Dt} = \mu_\alpha(\boldsymbol{\Gamma}\times\mathbf{B} + n_\alpha E) - D_\alpha \nabla n_\alpha \quad (1)$$

Here, α=±e ($\mu_\alpha = \frac{q_\alpha}{m_\alpha \nu_\alpha}$) is the mobility of electrons, ions and charged particles. Also, Γ shows the electron flux density. From the solution of this expression, the diffusion tensor is obtained as follows,

$$D = \begin{bmatrix} D_{xx\alpha} & D_{xy\alpha} & D_{xz\alpha} \\ D_{yx\alpha} & D_{yy\alpha} & D_{yz\alpha} \\ D_{zx\alpha} & D_{zy\alpha} & D_{zz\alpha} \end{bmatrix}. \tag{2}$$

For electrons and ions the elements of the tensor are as follows;

$$D_{xx\alpha} = K^{-1} D_\alpha \left[\omega_{cx\alpha}^2 + \nu_\alpha^2 \right] \qquad D_{xy\alpha} = K^{-1} D_\alpha \left[\omega_{cx\alpha}\omega_{cy\alpha} - \omega_{cz\alpha}\nu_\alpha \right]$$

$$D_{xz\alpha} = K^{-1} D_\alpha \left[-\omega_{cx\alpha}\omega_{cz\alpha} + \omega_{cy\alpha}\nu_\alpha \right] \quad D_{yx\alpha} = K^{-1} D_\alpha \left[\omega_{cx\alpha}\omega_{cy\alpha} - \omega_{cz\alpha}\nu_\alpha \right]$$

$$D_{yy\alpha} = K^{-1} D_\alpha \left[\omega_{cy\alpha}^2 + \nu_\alpha^2 \right] \qquad D_{yz\alpha} = -K^{-1} D_\alpha \left[\omega_{cy\alpha}\omega_{cz\alpha} + \omega_{cx\alpha}\nu_\alpha \right]$$

$$D_{zx\alpha} = -K^{-1} D_\alpha \left[\omega_{cx\alpha}\omega_{cz\alpha} + \omega_{cy\alpha}\nu_\alpha \right] \quad D_{zy\alpha} = K^{-1} D_\alpha \left[-\omega_{cy\alpha}\omega_{cz\alpha} + \omega_{cx\alpha}\nu_\alpha \right]$$

$$D_{zz\alpha} = K^{-1} D_\alpha \left[\omega_{cz\alpha}^2 + \nu_\alpha^2 \right] \qquad K = \left[\omega_{cx\alpha}^2 + \omega_{cy\alpha}^2 + \omega_{cz\alpha}^2 + \nu_\alpha^2 \right]$$

For ionosphere plasma, depending on the geometry of the Earth's magnetic field, if Eq. (1) is solved, the diffusion equations for unstable cases are given by including real and imaginary components;

$$D = \begin{bmatrix} D_{xxR} & D_{xyR} & D_{xzR} \\ D_{yxR} & D_{yyR} & D_{yzR} \\ D_{zxR} & D_{zyR} & D_{zzR} \end{bmatrix} + i \begin{bmatrix} D_{xxI} & D_{xyI} & D_{xzI} \\ D_{yxI} & D_{yyI} & D_{yzI} \\ D_{zxI} & D_{zyI} & D_{zzI} \end{bmatrix} \tag{3}$$

We can write the elements of this matrix in explicit form, step by step, in Eq. (4):

$$D_{xx\alpha R} = \frac{(\upsilon_\alpha^3(\upsilon_\alpha^2 + \omega_{c\alpha}^2 + \omega_{cx\alpha}^2 + 2\omega^2) + \upsilon_\alpha[\omega_{cx\alpha}^2(\omega_{c\alpha}^2 - 3\omega^2) + \omega^2(\omega_{c\alpha}^2 + \omega^2)]}{(\omega^2 + \upsilon_\alpha^2)[(\omega_{c\alpha}^2 + \upsilon_\alpha^2 - \omega^2) + 4\upsilon_\alpha^2\omega^2]}$$

$$D_{xx\alpha I} = \left[\frac{\upsilon_\alpha^2\omega\left(\upsilon_\alpha^2 - \omega_{c\alpha}^2 + 3\omega_{cx\alpha}^2 + 2\omega^2\right) + \omega\left(\omega_{c\alpha}^2 - \omega^2\right)\left(\omega_{cx\alpha}^2 - \omega^2\right)}{\left(\omega^2 + \upsilon_\alpha^2\right)\left[\left(\omega_{c\alpha}^2 + \upsilon_\alpha^2 - \omega^2\right) + 4\upsilon_\alpha^2\omega^2\right]} \right] \tag{4}$$

$$D_{xy\alpha R} = \frac{(\omega_{cx\alpha}\omega_{cy\alpha}\upsilon_\alpha\left(\omega_{c\alpha}^2+\upsilon_\alpha^2-3\omega^2\right)-\omega_{cz\alpha}\left(\upsilon_\alpha^2+\omega^2\right)\left(\omega_{c\alpha}^2+\upsilon_\alpha^2-\omega^2\right)}{(\omega^2+\upsilon_\alpha^2)[(\omega_{c\alpha}^2+\upsilon_\alpha^2-\omega^2)+4\upsilon_\alpha^2\omega^2]}$$

$$D_{xy\alpha I} = \left[\frac{(\omega_{cx\alpha}\omega_{cy\alpha}\omega\left(\omega_{c\alpha}^2+3\upsilon_\alpha^2-\omega^2\right)-2\omega_{cz\alpha}\upsilon_\alpha\omega\left(\upsilon_\alpha^2+\omega^2\right)}{\left(\omega^2+\upsilon_\alpha^2\right)\left[\left(\omega_{c\alpha}^2+\upsilon_\alpha^2-\omega^2\right)+4\upsilon_\alpha^2\omega^2\right]}\right]$$

$$D_{xz\alpha R} = \frac{-\omega_{cx\alpha}\omega_{cz\alpha}\upsilon_\alpha\left(\omega_{c\alpha}^2+\upsilon_\alpha^2-3\omega^2\right)-\omega_{cy\alpha}\left(\upsilon_\alpha^2+\omega^2\right)\left(\omega_{c\alpha}^2+\upsilon_\alpha^2-\omega^2\right)}{(\omega^2+\upsilon_\alpha^2)[(\omega_{c\alpha}^2+\upsilon_\alpha^2-\omega^2)+4\upsilon_\alpha^2\omega^2]}$$

$$D_{xz\alpha I} = \left[\frac{-\omega_{cx\alpha}\omega_{cz\alpha}\omega\left(\omega_{c\alpha}^2+3\upsilon_\alpha^2-\omega^2\right)-2\omega_{cy\alpha}\upsilon_\alpha\omega\left(\upsilon_\alpha^2+\omega^2\right)}{\left(\omega^2+\upsilon_\alpha^2\right)\left[\left(\omega_{c\alpha}^2+\upsilon_\alpha^2-\omega^2\right)+4\upsilon_\alpha^2\omega^2\right]}\right]$$

$$D_{yx\alpha R} = \frac{(\omega_{cx\alpha}\omega_{cy\alpha}\upsilon_\alpha\left(\omega_{c\alpha}^2+\upsilon_\alpha^2-3\omega^2\right)-\omega_{cz\alpha}\left(\upsilon_\alpha^2+\omega^2\right)\left(\omega_{c\alpha}^2+\upsilon_\alpha^2-\omega^2\right)}{(\omega^2+\upsilon_\alpha^2)[(\omega_{c\alpha}^2+\upsilon_\alpha^2-\omega^2)+4\upsilon_\alpha^2\omega^2]}$$

$$D_{yx\alpha I} = \left[\frac{(\omega_{cx\alpha}\omega_{cy\alpha}\omega\left(\omega_{c\alpha}^2+3\upsilon_\alpha^2-\omega^2\right)-2\omega_{cz\alpha}\upsilon_\alpha\omega\left(\upsilon_\alpha^2+\omega^2\right)}{\left(\omega^2+\upsilon_\alpha^2\right)\left[\left(\omega_{c\alpha}^2+\upsilon_\alpha^2-\omega^2\right)+4\upsilon_\alpha^2\omega^2\right]}\right]$$

$$D_{yy\alpha R} = \frac{(\upsilon_\alpha^3(\upsilon_\alpha^2+\omega_{c\alpha}^2+\omega_{cy\alpha}^2+2\omega^2)+\upsilon_\alpha[\omega_{cy\alpha}^2(\omega_{c\alpha}^2-3\omega^2)+\omega^2(\omega_{c\alpha}^2+\omega^2)]}{(\omega^2+\upsilon_\alpha^2)[(\omega_{c\alpha}^2+\upsilon_\alpha^2-\omega^2)+4\upsilon_\alpha^2\omega^2]}$$

$$D_{yy\alpha I} = \left[\frac{\upsilon_\alpha^2\omega\left(\upsilon_\alpha^2-\omega_{c\alpha}^2+3\omega_{cy\alpha}^2+2\omega^2\right)+\omega\left(\omega_{c\alpha}^2-\omega^2\right)\left(\omega_{cy\alpha}^2-\omega^2\right)}{\left(\omega^2+\upsilon_\alpha^2\right)\left[\left(\omega_{c\alpha}^2+\upsilon_\alpha^2-\omega^2\right)+4\upsilon_\alpha^2\omega^2\right]}\right]$$

$$D_{yz\alpha R} = -\frac{(\omega_{cy\alpha}\omega_{cz\alpha}\upsilon_\alpha\left(\omega_{c\alpha}^2+\upsilon_\alpha^2-3\omega^2\right)+\omega_{cx\alpha}\left(\upsilon_\alpha^2+\omega^2\right)\left(\omega_{c\alpha}^2+\upsilon_\alpha^2-\omega^2\right)}{(\omega^2+\upsilon_\alpha^2)[(\omega_{c\alpha}^2+\upsilon_\alpha^2-\omega^2)+4\upsilon_\alpha^2\omega^2]}$$

$$D_{yz\alpha I} = \left[\frac{(-\omega_{cy\alpha}\omega_{cz\alpha}\omega\left(\omega_{c\alpha}^2+3\upsilon_\alpha^2-\omega^2\right)+2\omega_{cx\alpha}\upsilon_\alpha\omega\left(\upsilon_\alpha^2+\omega^2\right)}{\left(\omega^2+\upsilon_\alpha^2\right)\left[\left(\omega_{c\alpha}^2+\upsilon_\alpha^2-\omega^2\right)+4\upsilon_\alpha^2\omega^2\right]}\right]$$

$$D_{zy\alpha R} = -\frac{(\omega_{cy\alpha}\omega_{cz\alpha}\upsilon_\alpha\left(\omega_{c\alpha}^2+\upsilon_\alpha^2-3\omega^2\right)+\omega_{cx\alpha}\left(\upsilon_\alpha^2+\omega^2\right)\left(\omega_{c\alpha}^2+\upsilon_\alpha^2-\omega^2\right)}{(\omega^2+\upsilon_\alpha^2)[(\omega_{c\alpha}^2+\upsilon_\alpha^2-\omega^2)+4\upsilon_\alpha^2\omega^2]}$$

$$D_{zy\alpha I} = \left[\frac{(-\omega_{cy\alpha}\omega_{cz\alpha}\omega\left(\omega_{c\alpha}^2+3\upsilon_\alpha^2-\omega^2\right)+2\omega_{cx\alpha}\upsilon_\alpha\omega\left(\upsilon_\alpha^2+\omega^2\right)}{\left(\omega^2+\upsilon_\alpha^2\right)\left[\left(\omega_{c\alpha}^2+\upsilon_\alpha^2-\omega^2\right)+4\upsilon_\alpha^2\omega^2\right]}\right]$$

$$D_{zx\alpha R} = \frac{-\omega_{cx\alpha}\omega_{cz\alpha}\upsilon_\alpha\left(\omega_{c\alpha}^2+\upsilon_\alpha^2-3\omega^2\right)-\omega_{cy\alpha}\left(\upsilon_\alpha^2+\omega^2\right)\left(\omega_{c\alpha}^2+\upsilon_\alpha^2-\omega^2\right)}{(\omega^2+\upsilon_\alpha^2)[(\omega_{c\alpha}^2+\upsilon_\alpha^2-\omega^2)+4\upsilon_\alpha^2\omega^2]}$$

$$D_{zx\alpha I} = \left[\frac{-\omega_{cx\alpha}\omega_{cz\alpha}\omega\left(\omega_{c\alpha}^2+3\upsilon_\alpha^2-\omega^2\right)-2\omega_{cy\alpha}\upsilon_\alpha\omega\left(\upsilon_\alpha^2+\omega^2\right)}{\left(\omega^2+\upsilon_\alpha^2\right)\left[\left(\omega_{c\alpha}^2+\upsilon_\alpha^2-\omega^2\right)+4\upsilon_\alpha^2\omega^2\right]}\right]$$

$$D_{zy\alpha R} = -\frac{(\omega_{cy\alpha}\omega_{cz\alpha}\upsilon_\alpha\left(\omega_{c\alpha}^2+\upsilon_\alpha^2-3\omega^2\right)+\omega_{cx\alpha}\left(\upsilon_\alpha^2+\omega^2\right)\left(\omega_{c\alpha}^2+\upsilon_\alpha^2-\omega^2\right)}{(\omega^2+\upsilon_\alpha^2)[(\omega_{c\alpha}^2+\upsilon_\alpha^2-\omega^2)+4\upsilon_\alpha^2\omega^2]}$$

$$D_{zy\alpha I} = \left[\frac{(-\omega_{cy\alpha}\omega_{cz\alpha}\omega\left(\omega_{c\alpha}^2+3\upsilon_\alpha^2-\omega^2\right)+2\omega_{cx\alpha}\upsilon_\alpha\omega\left(\upsilon_\alpha^2+\omega^2\right)}{\left(\omega^2+\upsilon_\alpha^2\right)\left[\left(\omega_{c\alpha}^2+\upsilon_\alpha^2-\omega^2\right)+4\upsilon_\alpha^2\omega^2\right]}\right]$$

$$D_{zz\alpha R} = \frac{(\upsilon_\alpha^3(\upsilon_\alpha^2+\omega_{c\alpha}^2+\omega_{cz\alpha}^2+2\omega^2)+\upsilon_\alpha[\omega_{cz\alpha}^2(\omega_{c\alpha}^2-3\omega^2)+\omega^2(\omega_{c\alpha}^2+\omega^2)]}{(\omega^2+\upsilon_\alpha^2)[(\omega_{c\alpha}^2+\upsilon_\alpha^2-\omega^2)+4\upsilon_\alpha^2\omega^2]}$$

$$D_{zz\alpha I} = \left[\frac{\upsilon_\alpha^2\omega\left(\upsilon_\alpha^2-\omega_{c\alpha}^2+3\omega_{cz\alpha}^2+2\omega^2\right)+\omega\left(\omega_{c\alpha}^2-\omega^2\right)\left(\omega_{cz\alpha}^2-\omega^2\right)}{\left(\omega^2+\upsilon_\alpha^2\right)\left[\left(\omega_{c\alpha}^2+\upsilon_\alpha^2-\omega^2\right)+4\upsilon_\alpha^2\omega^2\right]}\right]$$

3. Numerical Analysis and Results

Using Eqs. (1), (2), (3) and (4) the diffusion coefficients for the heights of the F-regions were computed as seasonal latitudes for the year 1990. By the agreed criteria, the IRI model was utilized to derive the ionospheric parameters that were used in the calculation [16]. We looked at the seasonal variation of Eq. (3) for the diffusion coefficients in ionospheric plasma concerning latitude at altitudes of 390, 410, 450, 500, 550 and 600 km (these heights are altitudes at which equatorial anomaly occurs at F^2-Region). Seasonal diffusion coefficients were found for both the stable Eq. (2) and unstable Eq. (3) scenarios for the critical heights of the F-region that were previously determined [17,18]. Next, each element of the diffusion tensor was examined for equinox days in local time by averaging the elements whose orders were the same under the conditions taken into consideration. Twice a year, there are equinox days when day and night are approximately equal in duration. The times throughout the Earth's orbit around the Sun when its axis is neither tilted toward nor away from the Sun are designated by these events [19]. Every year, the equinoxes fall on or around March 20 or 21 and September 22 or 23. The Earth's axis is neither tilted away from the Sun (as in winter) nor towards it (as in summer) during the equinoxes when the Sun

is directly overhead the equator of the Earth. For most places on Earth, this means that day and night last about equal amounts of time. At the vernal equinox, Figure 2 displays the local temporal fluctuation of diffusion coefficients for the conditions ω=0 and ω≠0. As a result, diffusion coefficients increase quickly in both stable and unstable states between around 1.00 and 5.00 local time, reach a maximum at precisely 6.00 o'clock, and then rapidly fall after this period. The terms ‘‘ω=0, $D_{xy}=D_{yx}$’’ refer to trigonometric exponential increases and decreases.

In terms of magnitudes, it can be listed as $D_{yy} > D_{xy} > D_{yz} > D_{xx} > D_{xz} > D_{zz}$. All values are approximately 10^8 (m^2/sec). However, looking at the same figure, the trend of change of diffusion coefficients for the ω≠0 condition is the same as for the unstable case, but their magnitude decreases dramatically. Among the tensor elements of the real part, the diagonal elements are larger and the other elements are smaller. The smallest value is D_{xzR} with a record low of 10^{-14} (m^2 / sec). As for the imaginary part, it takes the diagonal elements with higher values than other tensor elements. As for the imaginary part, it takes the diagonal elements with higher values than other tensor elements.

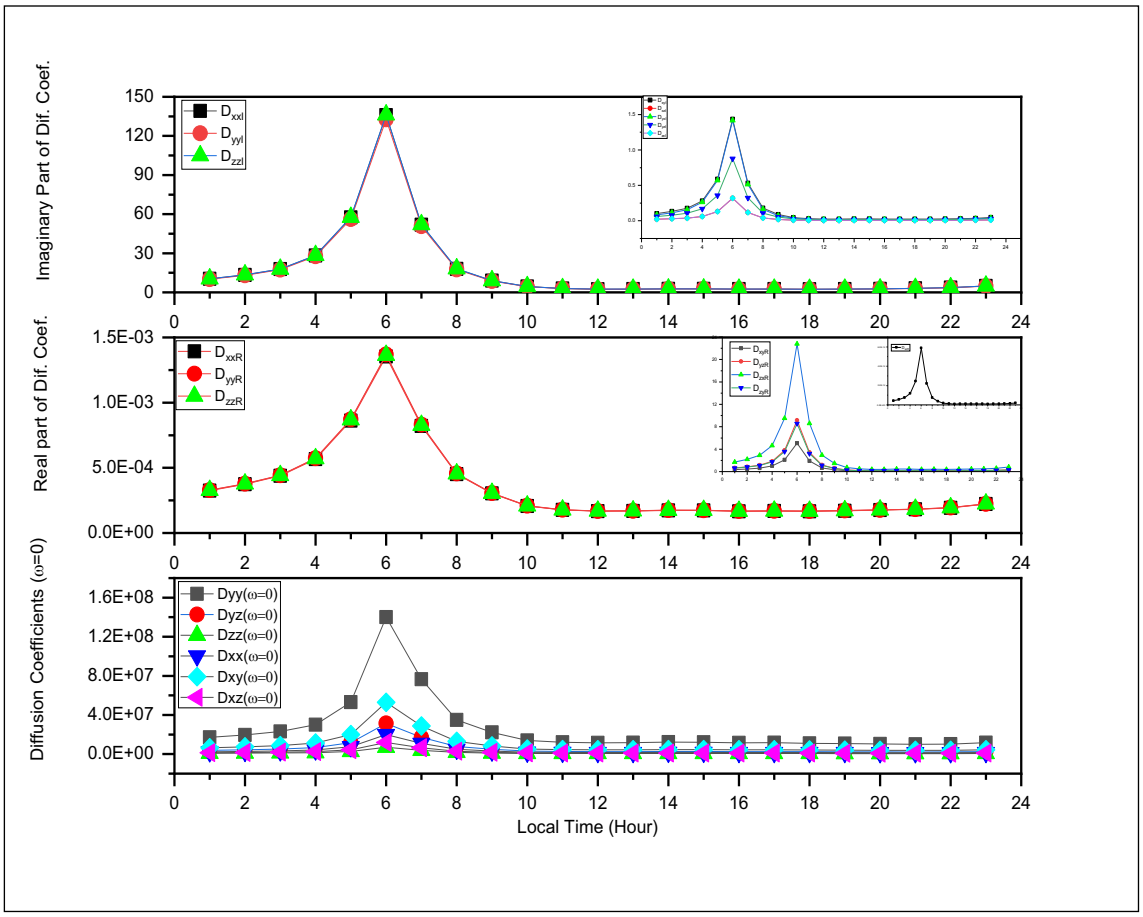

Figure 2. Variation of diffusion coefficients with local time for stable and unstable conditions at the equator (March. 21).

For the autumn equinox, the change of diffusion coefficients with local time under the considered conditions is given in Figure 3. The diagram is the same for the vernal equinox. In a steady state, the order according to the magnitude of the coefficients is $D_{xx} > D_{xy} > D_{xz} > D_{yy} > D_{yz} > D_{zx} > D_{zy} > D_{zz}$. There is no significant change in the magnitude of the diffusion coefficients during both equinoxes [20, 21]. They are almost equal to each other. In the steady state, the magnitudes of the diffusion coefficients are 10^8 m^2/sec, in the unstable state, the diagonal elements of the real part tensor of the diffusion coefficients are on the order of 10^{-4}, and other tensor elements outside the diagonal elements have values close to the magnitudes of the imaginary part tensor, except D_{xzR} [22, 23]. The diagonal elements of the imaginary part are the largest, and the other elements are 100 times smaller than their diagonal elements. Sizes vary between 0.5-150 m^2/sec.

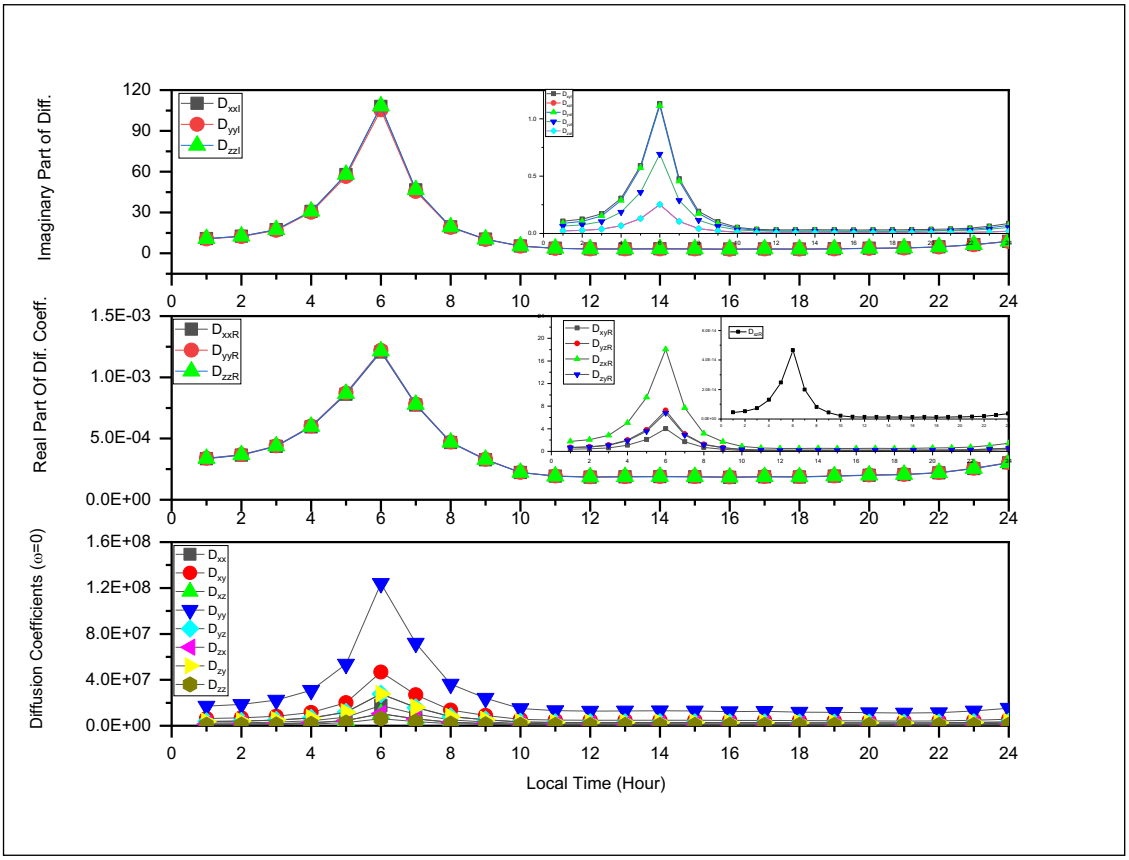

Figure 3. Variation of diffusion coefficients with local time for stable and unstable conditions at the equator (Sempt. 23).

4. Conclusion

This study aims to solve the diffusion equations, which are the most significant transport processes in the ionospheric plasma, analytically in both steady and unstable states. It does this by utilizing the northern hemisphere's actual magnetic field geometry and by applying these equations to specific conditions in the ionosphere to produce numerical results. Outcomes attained in the previously agreed circumstances

1- At six in the morning, all diffusion tensor elements, in both stable and unstable scenarios, reach their maximum.

2. Diffusion coefficients in steady state are around 10^8 (m^2/sec).

3. The real part's diagonal elements have sizes in the order of 10^{-4} (m^2/sec) in the unstable scenario.

4- The imaginary part's tensor elements in the unstable scenario range in magnitude from 0 to 150 m^2/sec.

The electron density of the ionosphere affects its properties, particularly the F region, which is crucial for radio wave reflection, propagation, and refraction. The conditions of reflection will alter if there is an anomaly in the electron density for whatever reason. The results of this study show that the electron density forms a peak and trough around the equator due to diffusion coefficients, which are responsible for phenomena like ‘‘equality of day and night,’’ ‘‘spring and autumn equinoxes,’’ and ‘‘vertical rays of the sun. ’’ The reflection height shortens on the hills and increases in the troughs as a result of these hills and troughs. Every diffusion coefficient exhibits this condition.

References

[1] Sağır S, Yeşil A. The relation between the refractive index of the equatorial ionospheric F2 region and long-term solar indices. Wirel Pers Commun 2018;102: 31-40.

[2] Yeşil A, Sağır S, Kurt K. The behavior of the classical diffusion tensor for equatorial ionospheric plasma. Journal of Science, 2016; 13: 123.

[3] Rishbeth H. Physics and chemistry of the ionosphere. Contemp Phys 1973;14(3): 229-249.

[4] Rishbeth H, Garriot OK. Introduction to Ionospheric Physics. New York, USA: Academic Press, 1969.

[5] Timoçin E, Yeşil A, Ünal İ. The effect of the geomagnetic activity to the hourly variations of ionospheric foF2 values at low latitudes. Arab J Geosci 2014; 7: 4437-4442.

[6] Kurt K. The Seasonal Behavior of the Characteristic Wave in Low Latitudes. Int J Innovative Eng Appl 2021; 5(1): 36-39.

[7] Mungufeni P, Rabiu BA, Okoh D, Jurua E. Characterisation of Total Electron Content over African region using Radio Occultation observations of COSMIC satellites. Adv Space Res 2020; 65(1): 19-29.

[8] Yesil A, Sagir S, Kurt K. The Behaviour of the Classical Diffusion Tensor for Equatorial Ionospheric Plasma. J Sci 2016; 13:123-127.

[9] Denisenko VV, Rycroft MJ, Harrison RG. A Mathematical Model of the Global Ionospheric Electric Field Generated by Thunderstorms. Bull Russ Acad Sci: Phys 2023; 87(1): 118-123.

[10] Tabassum A, Park K, Shin J, Jin HG, Baik JJ. Long-term changes in temperature, specific humidity, and precipitation in Bangladesh revealed by ERA5 data. Theor Appl Climatol 2023; 1-11.

[11] Olsen RC, Shawhan SD, Gallagher DL, Green JL, Chappell CR, Anderson RR. Plasma observations at the Earth's magnetic equator. J Geophys Res Space Phys 1987;92(A3): 2385-2407.

[12] Razzhevaikin VN. Instability of stationary nonmonotone solutions of the reaction equation with diffusion depending on density. Differ Equ 2006; 42: 567-575.

[13] Kolesnikov AF. Tirskii GA. The Stefan-Maxwell equations for diffusion fluxes of plasma in a magnetic field. Fluid Dyn 1985;19(4): 643–649.

[14] Yesil A. Sagir S. Kurt K. The Behaviour of the Classical Diffusion Tensor for Equatorial Ionospheric Plasma, J. Sci 2016; 13:123-127

[15] Timoçin E, Ünal İ, Yeşil A. The Effect of the midlatitude electron density trough on the ionospheric conductivities. Iran J Sci Technol Trans A: Sci 2019; 43: 297-307.

[16] Sağir S, Yaşar M, Atici R. The Relationship between Dst, IMF-Bz and collision parameters for $O^{+}+ N_2 \rightarrow NO^{+}+ N$ reactive scattering in the ionosphere. Geomagnetism and Aeronomy, 2019; 59: 1003-1008.

[17] Mendonça JT. Diffusion of magnetic field lines in a toroidal geometry. Phys Fluid Plasma Phys 1991; 3(1): 87-94.

[18] Kurt K, Yeşil MB. The Comparison of the Group and Phase Velocity of the Polarized Wave and the Equatorial Anomaly of the Ionosphere. Eur J Res Dev 2022; 2(2): 466-474.

[19] Katlamudi MR, Bulusu J. Low latitude Pi^2 pulsations at Desalpar, Gujarat, India: A statistical analysis of the influences of magnetic storms/substorms, seasons, and solar cycles. J Atmos Sol Terr Phys 2023; 252: 106145.

[20] Yeşil A, Sağır S. The New Diffusion Tensor and the Equatorial Anomaly Altitudes of F-Region. Celal Bayar Univ J. Sci 2017; 13(3): 717-723.

[21] Yasar M. The solar eclipse effect on diffusion processes of $O^{+}+ O_2 \rightarrow O_2^{+}+ O$ reaction for the upper ionosphere over Kharkov. Therm Sci, 2021; 25(1): 57-63.

[22] Ünal İ, Karatay S, Yeşil A, Hançerlioğulları A. Seasonal variations of impedance in the ionospheric plasma. 2020; J Polytech.

[23] Yasar M. The change of diffusion processes for $O^{+}+ N_2 \rightarrow NO^{+}+ N$ reaction in the ionospheric F region during the solar eclipse over Kharkov. Therm Sci 2021; 25(1): 51-56.